

## Article

# Improving the Flotation of Unoxidized and Oxidized Molybdenite Fines Using Dodecylamine as a Collector: Flotation Tests and Interaction Mechanism

Bingqiao Yang <sup>1,2,3,\*</sup>, Jie Wu <sup>4,5,\*</sup>, Bing Deng <sup>1</sup> , Hui Shao <sup>3</sup>, Shaoxian Song <sup>5</sup> and Mildred Quintana <sup>6</sup> 

<sup>1</sup> Technology Innovation Center for Comprehensive Utilization of Strategic Mineral Resources, Ministry of Natural Resources, Chengdu 610041, China; dbing@mail.cgs.gov.cn

<sup>2</sup> Hubei Three Gorges Laboratory, Yichang 443008, China

<sup>3</sup> School of Resources and Safety Engineering, Wuhan Institute of Technology, Wuhan 430073, China; shaohuivs@163.com

<sup>4</sup> Doctorado Institucional de Ingeniería y Ciencia de Materiales, Universidad Autonoma de San Luis Potosi, Av. Sierra Leona 530, San Luis Potosi 78210, Mexico

<sup>5</sup> School of Resources and Environmental Engineering, Wuhan University of Technology, Wuhan 430070, China; ssx851215@whut.edu.cn

<sup>6</sup> Facultad de Ciencias, Universidad Autonoma de San Luis Potosi, Av. Parque Chapultepec 1570, San Luis Potosi 78210, Mexico; quintanamildred@gmail.com

\* Correspondence: bqyang@wit.edu.cn (B.Y.); abbyduola@163.com (J.W.)

**Abstract:** The flotation of unoxidized and oxidized molybdenite fines is a challenging job worldwide. In this work, dodecylamine (DDA) was developed as a potential collector to improve the flotation of molybdenite fines with and without oxidation. The flotation behaviors and interaction mechanisms were probed through flotation tests, contact angle, Zeta potential, Scanning Electron Microscope-Energy Dispersive Spectrometer (SEM-EDS), and X-ray Photoelectron Spectroscopy (XPS). The flotation tests revealed that DDA improved the flotation of unoxidized or oxidized molybdenite fines efficiently. The results of Zeta potential, contact angle, and SEM-EDS uncovered that a substantial number of DDA species adsorbed on both fresh and oxidized molybdenite faces and edges, thus enhancing their hydrophobicity. XPS analysis further manifested that  $\text{RNH}_2$  and  $\text{RNH}_3^+$  adsorbed on the S atoms of fresh faces through hydrogen bonding. Meanwhile,  $\text{RNH}_2$  and  $\text{RNH}_3^+$  mainly adsorbed on fresh edges via chemical bonding between amine groups and Mo sites and electrostatic force. For oxidized molybdenite,  $\text{RNH}_2$  and  $\text{RNH}_3^+$  interacted with oxidized faces through hydrogen bonding while adsorbed on oxidized edges via hydrogen bonding and electrostatic interaction.

**Keywords:** molybdenite fines; face and edge; flotation; dodecylamine; oxidation



**Citation:** Yang, B.; Wu, J.; Deng, B.; Shao, H.; Song, S.; Quintana, M. Improving the Flotation of Unoxidized and Oxidized Molybdenite Fines Using Dodecylamine as a Collector: Flotation Tests and Interaction Mechanism. *Minerals* **2024**, *14*, 468. <https://doi.org/10.3390/min14050468>

Academic Editor: Luis Vinnett

Received: 30 March 2024

Revised: 24 April 2024

Accepted: 26 April 2024

Published: 28 April 2024



**Copyright:** © 2024 by the authors. Licensee MDPI, Basel, Switzerland. This article is an open access article distributed under the terms and conditions of the Creative Commons Attribution (CC BY) license (<https://creativecommons.org/licenses/by/4.0/>).

## 1. Introduction

Molybdenum (Mo) is a rare and strategic metal that has been broadly used in the metallurgy, machinery, chemical, and aerospace industries owing to its high strength and excellent corrosion resistance [1,2]. Up to now, 95% of molybdenum production originates from molybdenite. With the gradual reduction of high-grade molybdenite ores, exploiting fine-disseminated and low-grade molybdenite deposits is essential to satisfy increasing consumption demand. Nevertheless, these refractory ores are required to be finely ground to liberate them from other gangue minerals. As a laminar mineral with distinct anisotropic properties, molybdenite possesses polar edges and non-polar faces [3]. The hydrophilic edge originates from the cleavage of S–Mo covalent bonds, while the hydrophobic face is derived from the break of van der Waals force between S–Mo–S layers [4]. Notably, molybdenite hydrophobicity depends on the edge/face ratio. As particle size decreases, the hydrophilic edge gradually dominates, leading to a significant decline in the floatability of molybdenite fines [5].

In addition, oxidation is another important factor affecting the flotation of molybdenite ores. Molybdenite ores are prone to be oxidized in the presence of oxygen, moisture, microbial activity, and acidic substances [6], leading to diminishing hydrophobicity. [7]. Yi et al. reported that the oxidation reaction made the molybdenite surface less hydrophobic [8]. Wei et al. further revealed that both faces and edges exhibited hydrophilic properties after oxidation [9]. Because covalent bonds are ruptured to produce edges, they are known to be considerably more reactive than faces. As a result, the oxidation reaction occurs primarily on edges, and on the defect sites in faces [10]. Notably, molybdenite fines are more readily oxidized due to the dominant edges, and then the hydrophobicity significantly decreases, resulting in the poor flotation performance of oxidized molybdenite fines.

Kerosene is a commonly used collector for molybdenite flotation that preferentially adsorbs on molybdenite faces rather than edges via van der Waals forces and hydrophobic interactions [11]. However, kerosene cannot efficiently collect molybdenite fines owing to its poor affinity toward hydrophilic edges. After oxidation, since the hydrophobicity of the faces decrease, the affinity between kerosene and the faces becomes weaker, leading to worse floatability. Consequently, exploring novel collectors to improve the flotation of oxidized and unoxidized molybdenite fines is essential.

Dodecylamine (DDA) is a common cationic collector, which can be used to collect silicate and oxidized minerals. In its molecular structure, DDA contains a long carbon chain and an amine group. The amine group has a lone-pair electron that can complex with metal sites. Meanwhile, the long carbon chain renders the mineral surface hydrophobic. In this work, DDA was first tested as a collector of molybdenite fines. The flotation performances and interaction mechanisms were probed via flotation, contact angle, Zeta potential, SEM-EDS, and XPS measurements. The objective was to verify if it was suitable for promoting the flotation of molybdenite fines and to shed some light on its interaction mechanism.

## 2. Experimental

### 2.1. Materials

Molybdenite samples were purchased from Guangxi province, China. These samples were selected, ground, and screened to obtain  $-20\ \mu\text{m}$  size fractions for flotation tests and measurements. The XRD (D8 Advance, Bruker, Billerica, MA, USA) pattern of molybdenite is illustrated in Figure 1, and there was no apparent impurity peak. The results of XRD and the chemical assay showed that the molybdenite samples were of high purity (97%).

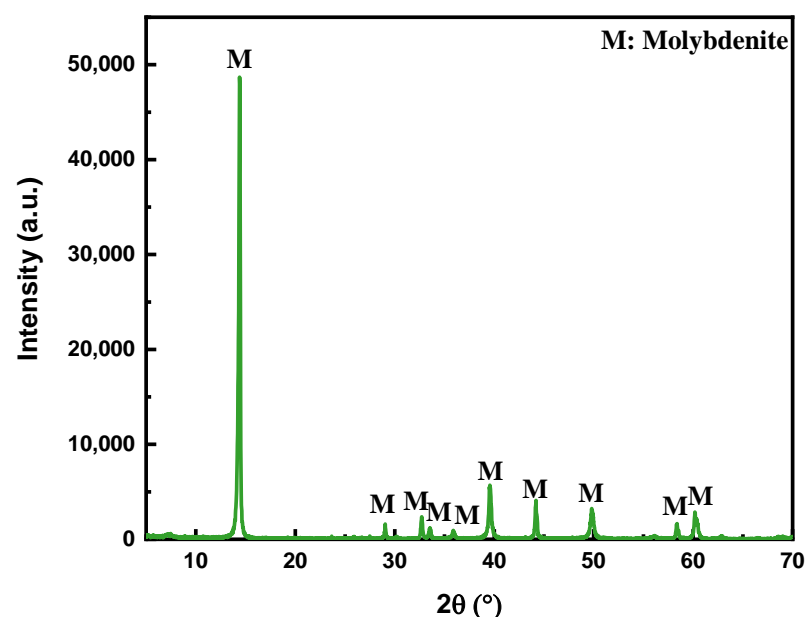


Figure 1. XRD pattern of raw mineral samples.

Reagents utilized in this work include the collectors DDA and kerosene, pH modifiers NaOH and HCl, the frother methyl isobutyl carbinol (MIBC), and oxidant hydrogen peroxide ( $\text{H}_2\text{O}_2$ ), which were all obtained from Aladin, China. Ultrapure water was used.

### 2.2. Oxidation Treatment and Flotation Tests

Molybdenite powders (2 g) were added to 1 M  $\text{H}_2\text{O}_2$  (30% *v/v*) solution, and the suspension was stirred at 300 rpm for 24 h. Then, the pulp was transferred to a flotation cell. After pH adjustment, DDA or kerosene was introduced and conditioned for 5 min. When kerosene was employed as the collector, MIBC was introduced to the pulp and conditioned for 1 min before flotation. When DDA was used as a collector, MIBC was not needed. The flotation was performed for three minutes.

### 2.3. Contact Angle Measurement

A contact angle goniometer (Dataphysics OCA20, Filderstadt, Germany) was employed to measure the contact angles of the face and edge samples using the sessile drop method. During the measurements, the needle with a diameter of 0.5 mm was used to inject ultrapure water droplets, resulting in a droplet size of about 4 mm. The bulk molybdenite with good crystallinity was used to prepare the faces and edges samples. The fresh faces ( $0.5 \times 0.5 \text{ cm}^2$ ) were obtained by mechanically exfoliating the top layers of molybdenite utilizing Scotch tape. An approximate 0.5 cm thick molybdenite sample was cut into  $0.4 \times 0.3 \text{ cm}^2$  for preparing the edges sample. The edges sample were polished with wet silicon carbide paper in the sequence of 240, 400, 800, 1200, 3000, and 7000 grit, and then polished with 1 and 0.3  $\mu\text{m}$  alumina powder suspensions, respectively. Moreover, the fresh faces and edges were immersed in  $\text{H}_2\text{O}_2$  solution for 24 h to prepare the oxidized faces and edges samples. For the treated samples with DDA, the fresh and oxidized faces and edges were immersed in 100 mg/L DDA solution (pH = 7) for 5 min. Afterwards, these samples were blown dry for measurement.

### 2.4. Zeta Potential Measurement

Zeta potential was measured using a Zetasizer Nano (Malvern, UK). First, 0.1 g oxidized or unoxidized molybdenite samples were added into a DDA solution (100 mg/L,  $10^{-3}$  M NaCl) and stirred for 5 min. After pH regulation, 1 mL of suspension was taken for measurements.

### 2.5. SEM-EDS Measurement

Molybdenite faces and edges samples were prepared as presented in Section 2.3. SEM (JEM-2100F, JEOL, Tokyo, Japan) was used to observe the morphology characteristics. The element distribution was detected with an Energy Dispersive Spectrometer (EDAX Elite, Pleasanton, CA, USA).

### 2.6. Raman Measurement

Raman spectra were obtained using an INVIA Raman microscope with a 532 nm Ar laser (Renishaw, Gloucestershire, UK). The faces and edges samples with and without oxidation were prepared as presented in Section 2.3. Moreover, the  $\text{H}_2\text{O}_2$  solution remaining after oxidation of the faces and edges was also used for measurements.

### 2.7. XPS Measurement

First, 2 g of unoxidized and oxidized molybdenite samples were treated with DDA solution (100 mg/L, pH = 7) and conditioned for 5 min. Then, the samples were collected and dried for measurements. XPS spectra were obtained by an X-ray photoelectron spectrometer (Thermo Scientific K-Alpha, Waltham, MA, USA). The measurement was conducted via an Al  $K\alpha$  sputtering ray source at 12 kV and pass energy of 50 eV. The spectra were fitted using Avantage software 5.9922. The standard C 1s peak was calibrated to 284.80 eV.

### 3. Results and Discussion

#### 3.1. Flotation Tests

Figure 2a presents the floatability of molybdenite fines as a function of pH. It was clear that molybdenite floatability decreased gradually as pH increased, which might be due to the generation of hydrophilic molybdate ions [12]. After the addition of DDA, the floatability of molybdenite fines surged to 97% at a pH of 5, whereas a high dosage of kerosene achieved a floatability of 88.82%. Compared with kerosene, a lower dosage of DDA could achieve higher floatability, indicating that DDA was more efficient in the flotation of molybdenite fines at a broad pH range.

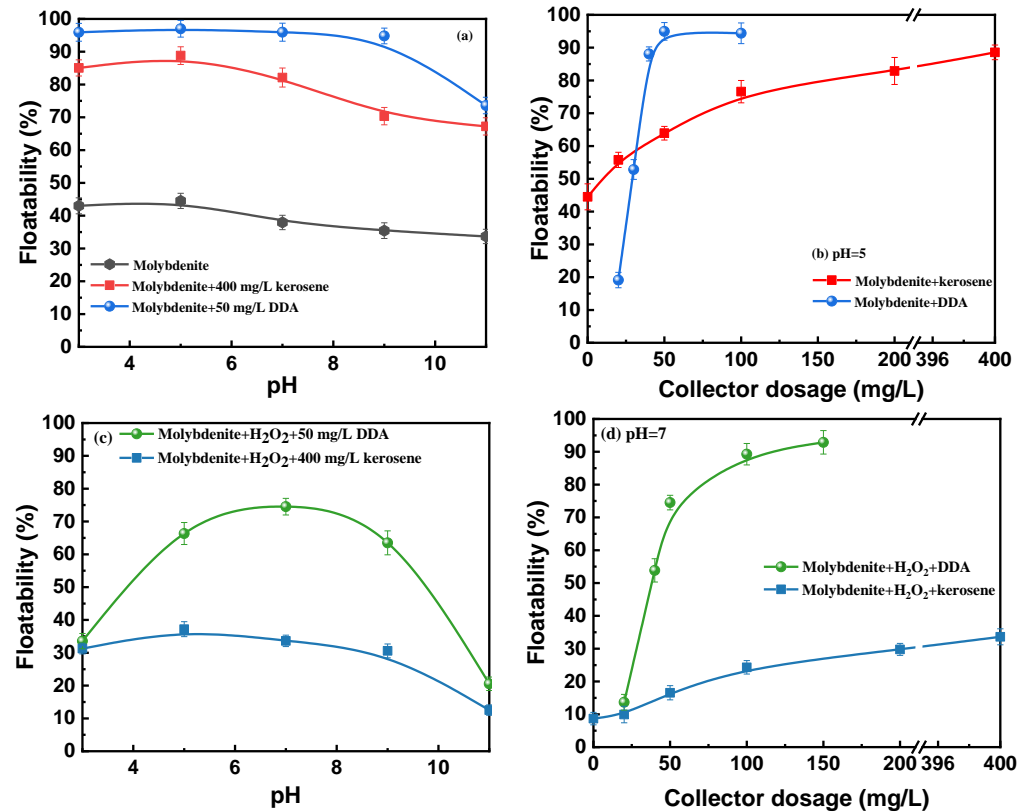


**Figure 2.** The influence of pH and collector dosage on the floatability of unoxidized (a,b) or oxidized (c,d) molybdenite fines.

Figure 2b shows the impact of collector dosage on the floatability of molybdenite fines. Notably, molybdenite floatability improved remarkably as the collector dosage increased. At DDA dosage of 50 mg/L, the floatability reached 94.96%, which was much higher than that (88.56%) obtained at kerosene dosage of 400 mg/L. These results revealed that DDA exhibited much stronger collecting ability to molybdenite fines, which had the potential to replace kerosene.

Figure 2c illustrates molybdenite floatability after oxidation as a function of pH. When kerosene was used as a collector, the floatability of oxidized molybdenite fines decreased slightly as pH increased. On the contrary, the floatability improved substantially after the introduction of DDA at a pH of 5–7. It was clear that a low dosage of DDA achieved floatability of 74.52% while a high dosage of kerosene only obtained floatability of 33.62% at a pH of 7. The huge difference in floatability meant that less reagent was needed when DDA was used. These results indicated that DDA also significantly improved the flotation of oxidized molybdenite fines.

The influence of collector dosage on the flotation of oxidized molybdenite fines is presented in Figure 2d. It was obvious that oxidized molybdenite exhibited very poor floatability (8.69%). After the addition of kerosene, the floatability reached 33.62% at

400 mg/L of kerosene. Notably, the floatability surged dramatically to nearly 90% when 100 mg/L of DDA was introduced. These results indicated that DDA was more effective than kerosene in collecting oxidized molybdenite fines.

### 3.2. Contact Angle

Figure 3 depicts contact angles of treated and untreated faces and edges under various conditions. The contact angle of fresh molybdenite faces and edges was  $76.5^\circ$  and  $42.5^\circ$ , respectively. After adding DDA, the contact angle of the faces and edges increased to  $89^\circ$  and  $86^\circ$ , suggesting that DDA improved the hydrophobicity of fresh faces and edges. After oxidation, the contact angle of both the faces and edges reduced to  $38.5^\circ$  and  $20^\circ$ , which explained the poor flotation of oxidized molybdenite fines. For oxidized molybdenite fines treated with DDA, the contact angle of the faces and edges reached  $88^\circ$  and  $80^\circ$ , respectively, which elucidated that DDA could also remarkably enhance the hydrophobicity of both oxidized faces and edges. These results revealed that DDA could improve the hydrophobicity of the faces and edges before and after oxidation, which corresponded well with the flotation results.

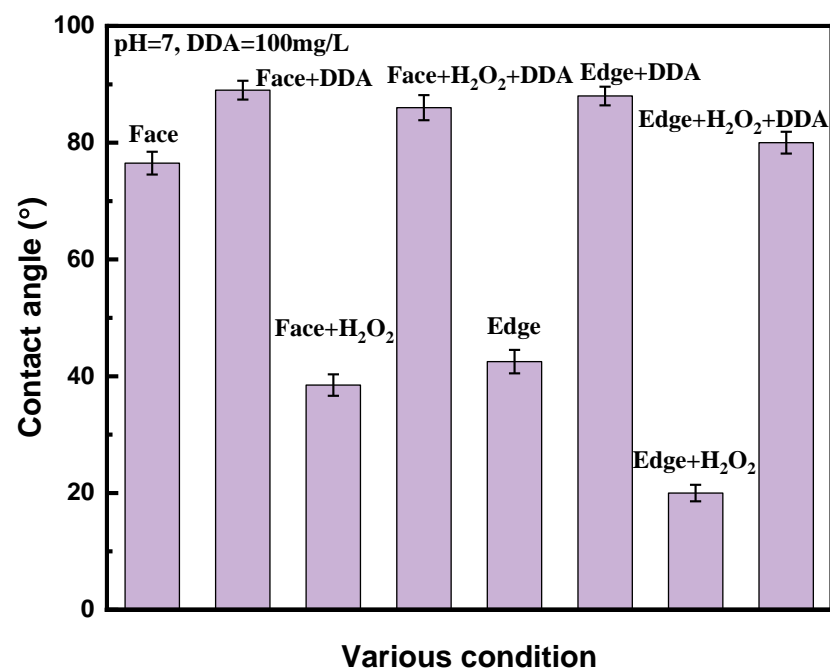
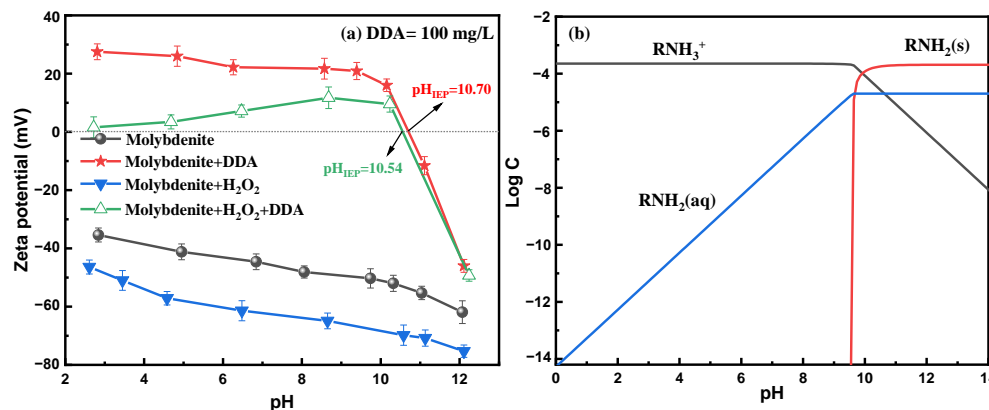


Figure 3. Contact angles of the molybdenite faces and edges under various conditions.

### 3.3. Zeta Potential

The effect of pH on Zeta potential of oxidized and unoxidized molybdenite fines with and without DDA is displayed in Figure 4a. For molybdenite, Zeta potential was negative throughout the pH range. After oxidation, Zeta potential shifted towards a more negative direction over the pH range, which might be ascribed to the formation of more negatively charged molybdate ions ( $\text{HMoO}_4^-/\text{MoO}_4^{2-}$ ) [7]. After the introduction of DDA, Zeta potential of both oxidized and unoxidized molybdenite fines became positive at a pH around 2–10, and their isoelectric point (IEP) moved to an approximate pH of 10.54 and 10.70, respectively. Based on the DDA species distribution diagram (Figure 4b), the cationic species  $\text{RNH}_3^+$  dominated, where a few neutral species of  $\text{RNH}_2(\text{aq})$  were also present in the pH range of 0–9.54. Consequently, it was easy to understand that these DDA species adsorbed on unoxidized and oxidized molybdenite surfaces and reversed their Zeta potential from negative to positive [13].



**Figure 4.** Zeta potential of treated and untreated molybdenite fines (a), DDA species distribution (b) as a function of pH.

### 3.4. Raman and SEM-EDS Analysis

The species of molybdenite faces and edges were examined using Raman spectrum. Figure 5a depicts Raman spectra of faces and edges before and after oxidation. The distinct peaks at 380 and 405  $\text{cm}^{-1}$  represented the in-plane  $E_{2g}^1$  and out-of-plane  $A_{1g}$  vibration modes of Mo-S bonds [14], which were detected on both unoxidized faces and edges. For oxidized edges, a new peak at 285  $\text{cm}^{-1}$  appeared, which was ascribed to  $\text{MoO}_3$ , indicating that the oxidation degree of the edges increased. For oxidized faces, the  $A_{1g}$  peak was broadened, suggesting the softening of the Mo-S phonon mode, which might be due to the decrease in Mo-S bonds [15]. Furthermore, both faces and edges exhibited red shifts of  $E_{2g}^1$  and  $A_{1g}$  peaks after oxidation, which might be due to the generation of sulfur vacancies during oxidation [16].

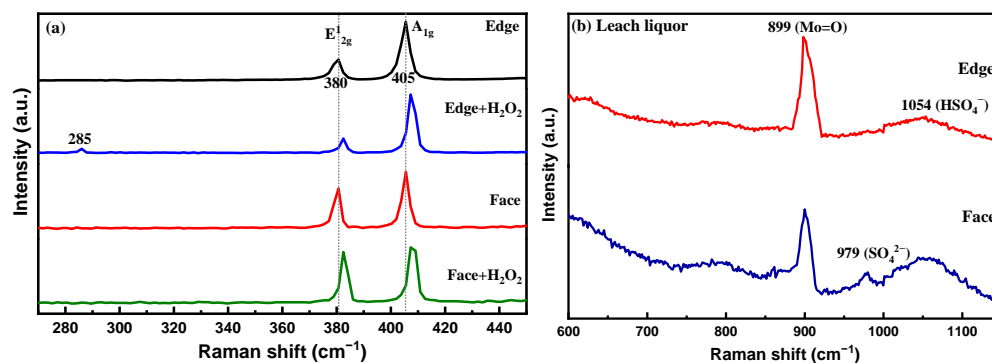


**Figure 5.** The Raman spectra of molybdenite faces and edges with and without  $\text{H}_2\text{O}_2$  treatment (a), oxidation leach liquor (b).

Raman spectra of molybdenite species in oxidation leach liquor are displayed in Figure 5b. For the edge liquor, the peaks at 899 and 1054  $\text{cm}^{-1}$  represented Mo=O in  $\text{MoO}_4^{2-}$  and  $\text{HSO}_4^-$ . For the face liquor, the same two peaks were also detected, and another peak at 979  $\text{cm}^{-1}$  of the faces was ascribed to  $\text{SO}_4^{2-}$  [17]. The appearance of  $\text{HSO}_4^-$  and  $\text{SO}_4^{2-}$  indicated the oxidation of sulfur in molybdenite. Compared with the edge liquor, the intensity of  $\text{MoO}_4^{2-}$  reduced while  $\text{HSO}_4^-$  increased in the face liquor, and the new peak of  $\text{SO}_4^{2-}$  appeared, indicating that more sulfur and fewer molybdenum oxidized products dissolved from faces than edges. Furthermore, ICP results illustrated that the sulfur and molybdenum elemental contents were 1016.84 mg/L and 330.03 mg/L in the liquor, suggesting the oxidized products of sulfur were more soluble than those of molybdenum.

Figure 6 and Table 1 present the SEM images and elemental atomic concentration of fresh and oxidized molybdenite faces and edges. The fresh faces and edges surfaces were

smooth and O content was relatively low. After oxidation, many hexagonal defects formed on faces. Meanwhile, the EDS results showed that the S and Mo content decreased slightly while the O content increased around these defects. Therefore, it was reasonable to deduce that the oxidation mainly caused the generation of defects on faces. For oxidized edges, large white oxides were observed. EDS analysis indicated that these oxides were primarily molybdenum oxide. Combined with Raman results, the broadened  $A_{1g}$  peak and red shift further demonstrated that these defects on oxidized faces might be sulfur vacancies, and the deposited molybdenum oxide on oxidized edges could be ascribed to  $MoO_3$ .

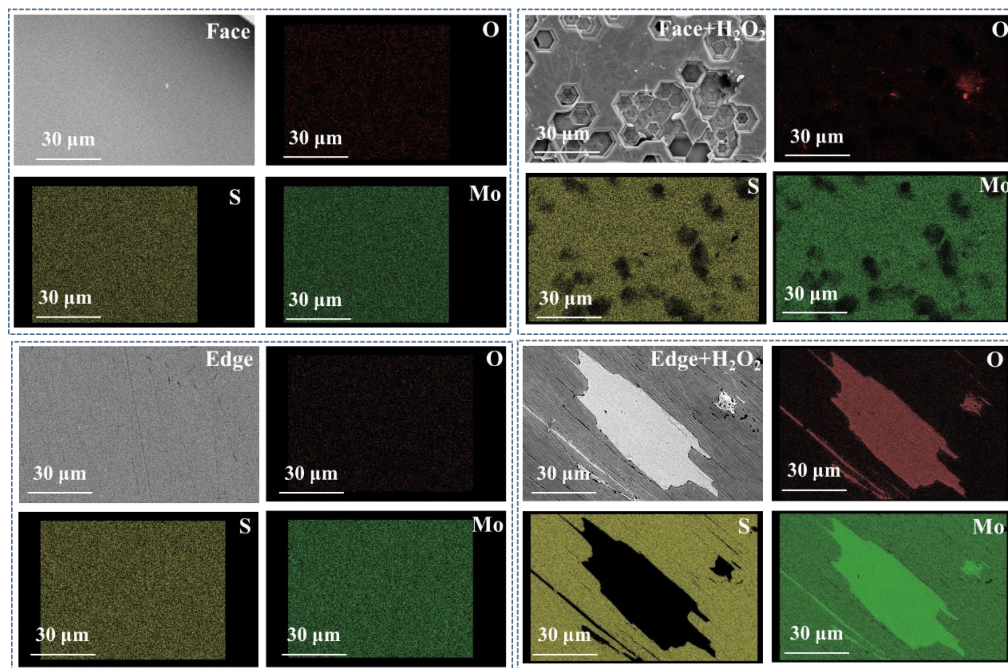
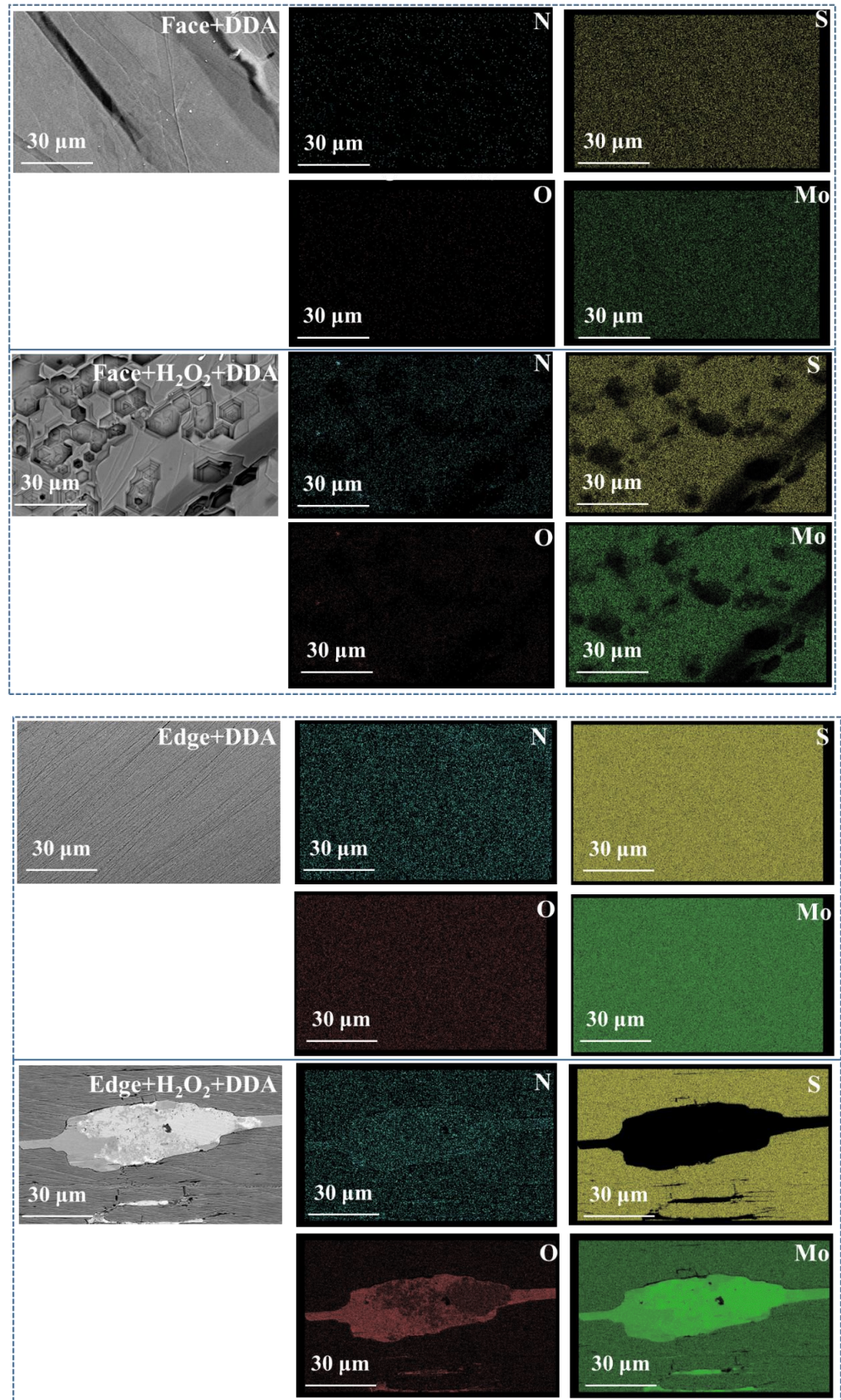


Figure 6. SEM-EDS images of molybdenite faces and edges before and after oxidation.

Table 1. Elemental atomic concentration of the face and edge with and without oxidation.

Surface	Oxidation State	Element Atomic Conc.		
		S	Mo	O
Face	Before	59.417	37.121	2.462
	After	57.568	36.937	5.495
Edge	Before	59.278	37.258	3.464
	After	31.736	50.530	17.734

The effect of DDA on oxidized and unoxidized faces and edges was also investigated by SEM-EDS. The photographs and element atomic concentration are displayed in Figure 7 and Table 2. Notably, a lot of the N element was detected on both fresh and oxidized faces and edges, suggesting DDA species adsorbed onto fresh and oxidized faces and edges, which was consistent with the contact angle results. Furthermore, the N atom concentration on oxidized faces and edges was higher than fresh faces and edges, which implied that DDA species were more readily adsorbed on the oxidized face and edge. Therefore, DDA species enhanced the hydrophobicity of the fresh and oxidized faces and edges, thus improving the floatability of unoxidized and oxidized molybdenite fines, which was in line with the contact angle result.



**Figure 7.** SEM-EDS images of fresh and oxidized molybdenite faces and edges in the absence and presence of DDA.

**Table 2.** Elemental atomic concentration of oxidized and unoxidized molybdenite faces and edges with and without DDA treatment.

Surface	Oxidation State	Element Atomic Conc.			
		S	Mo	O	N
Face	Before	59.417	37.121	2.462	0.798
	After	57.568	36.937	5.495	1.173
Edge	Before	61.212	37.895	0.344	0.549
	After	26.880	61.514	9.125	2.481

3.5. XPS Analysis

The XPS spectra of Mo 3d, S 2p, N 1s, and O 1s are shown in Figure 8. The peak binding energy and atomic concentration are listed in Table 3. In Figure 8a, the peak at 226.72 eV represented S 2s. The peaks at 229.37, 230.22, and 231.88 eV were ascribed to the Mo 3d<sub>5/2</sub> of MoS<sub>2</sub>, MoO<sub>2</sub>, and MoO<sub>3</sub>. The peaks at 232.52, 233.57, and 235.17 eV were attributed to the Mo 3d<sub>3/2</sub> of MoS<sub>2</sub>, MoO<sub>2</sub>, and MoO<sub>3</sub>, respectively [12]. After adding DDA, the peak of MoS<sub>2</sub> moved by approximately 0.33 eV, elucidating that DDA species might adsorb on the Mo sites of molybdenite. After oxidation, it was clear that the MoO<sub>3</sub> concentration greatly increased from 7.672% to 21.7% and the MoO<sub>2</sub> concentration slightly increased from 4.79% to 8.04%. For oxidized molybdenite treated with DDA, the movement of MoS<sub>2</sub> was 0.24 eV, while the movements of MoO<sub>2</sub> (0.09 eV) and MoO<sub>3</sub> (0.05 eV) were insignificant, implying that DDA species might chemisorb on MoS<sub>2</sub> but physisorb on MoO<sub>3</sub> and MoO<sub>2</sub>.

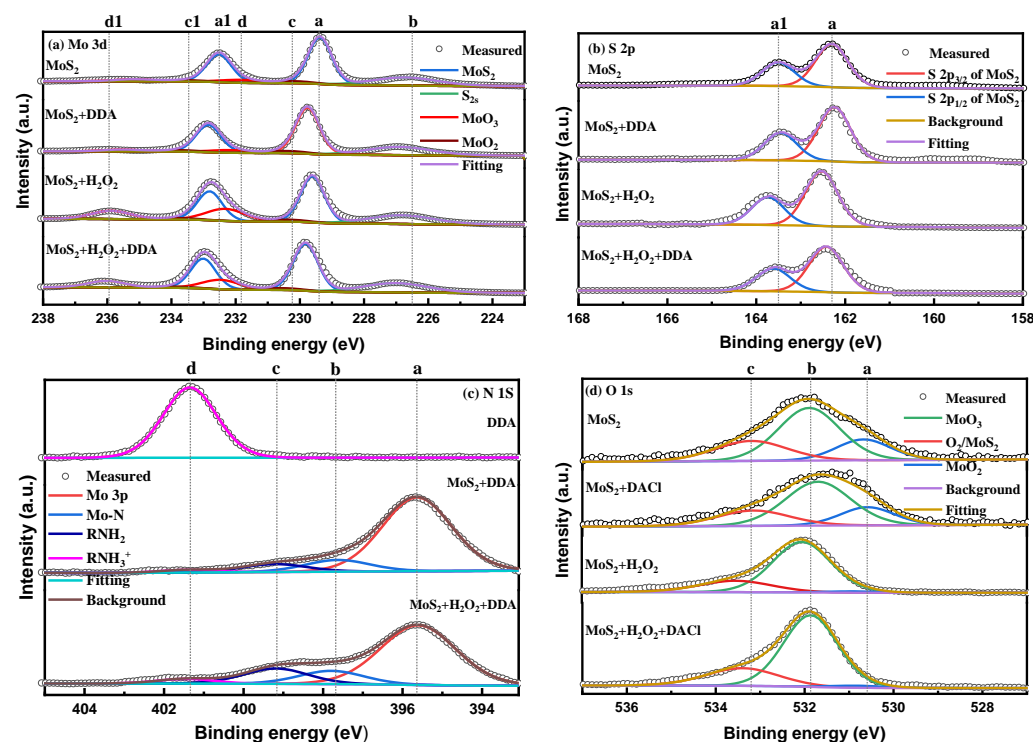


**Figure 8.** XPS spectra of Mo 3d (a), S 2p (b), N 1s (c), and O 1s (d) for treated and untreated molybdenite fines.

**Table 3.** Fitting parameters of XPS spectra.

Orbital	Species	Untreated		+DDA		+H <sub>2</sub> O <sub>2</sub>		+H <sub>2</sub> O <sub>2</sub> +DDA	
		BE	AC	BE	AC	BE	AC	BE	AC
Mo 3d	a(MoS <sub>2</sub> )	229.37	40.58	229.70	41.64	229.61	32.71	229.85	33.89
	a1(MoS <sub>2</sub> )	232.52	28.07	232.85	26.13	232.81	21.81	233.05	23.4
	b(S <sub>2s</sub> )	226.72	19.31	226.90	20.33	226.83	15.75	277.01	18.39
	c(MoO <sub>2</sub> )	230.22	2.83	230.43	2.97	230.40	4.82	230.49	4.69
	c1(MoO <sub>2</sub> )	233.57	1.96	233.74	2.05	233.75	3.22	233.86	3.24
	d(MoO <sub>3</sub> )	231.88	4.29	232.19	4.06	232.32	13.02	232.47	9.68
	d1(MoO <sub>3</sub> )	235.17	2.97	233.54	2.81	235.88	8.68	236.03	6.7
S 2p	a(S 2p <sub>3/2</sub> )	162.30	64.53	162.24	66.19	162.53	66.19	162.42	66.61
	a1(S 2p <sub>1/2</sub> )	163.50	35.37	163.45	33.81	163.74	33.81	163.63	33.39
N 1s	a(Mo <sub>3p</sub> )	-	-	395.64	75.98	-	-	395.60	68.05
	b(Mo-N)	-	-	397.63	13.74	-	-	397.79	14.62
	c(RNH <sub>2</sub> )	-	-	399.22	8.25	-	-	399.19	12.71
	d(RNH <sub>3</sub> <sup>+</sup> )	401.35	100	401.42	2.02	-	-	401.45	4.63
O 1s	a(MoO <sub>2</sub> )	530.68	19.47	530.59	19.94	530.94	1.88	530.87	2.18
	b(MoO <sub>3</sub> )	531.85	55.69	531.70	57.65	532.06	76.61	531.86	73.63
	c(O <sub>2</sub> /MoS <sub>2</sub> )	533.20	24.84	533.15	22.41	533.55	21.51	533.40	24.18

BE—bind energy (eV), AC—atomic concentration (%), “-” denotes none.

In S 2p spectra (Figure 8b), for untreated molybdenite, the peaks centered at 162.30 and 163.50 eV, which denoted S 2p<sub>3/2</sub> and S 2p<sub>1/2</sub> of MoS<sub>2</sub> [18]. For the oxidized molybdenite, the S 2p<sub>3/2</sub> and S 2p<sub>1/2</sub> of MoS<sub>2</sub> shifted to 162.53 and 163.74 eV. After the addition of DDA, the peaks of both unoxidized and oxidized molybdenite moved slightly to a lower binding energy. It has been reported that the sulfur atom was prone to form H bonds with RNH<sub>2</sub> and RNH<sub>3</sub><sup>+</sup> species [19,20]. Thus, it was safe to say that the decrease in binding energy might be attributed to hydrogen bonding.

In Figure 8c, the peak at 401.35 eV represented RNH<sub>3</sub><sup>+</sup> of DDA [19]. For molybdenite treated with DDA, the peaks at 395.64, 397.63, 399.22, and 401.42 eV denoted Mo 3p of MoS<sub>2</sub> [4], Mo-N [21], RNH<sub>2</sub> [22], and RNH<sub>3</sub><sup>+</sup>. The same peaks were also detected on the oxidized molybdenite treated with DDA, which centered at 395.60, 397.79, 399.19, and 401.45 eV, respectively. The appearance of RNH<sub>2</sub> and RNH<sub>3</sub><sup>+</sup> demonstrated that DDA species adsorbed on both unoxidized and oxidized molybdenite surfaces [23]. Meanwhile, the appearance of the Mo-N bond might imply the formation of a molybdenum-amine complex ion, in which the RNH<sub>2</sub> bonded with the Mo sites [19]. In addition, the higher RNH<sub>2</sub> and RNH<sub>3</sub><sup>+</sup> concentrations on oxidized molybdenite compared to unoxidized molybdenite suggested that RNH<sub>2</sub> and RNH<sub>3</sub><sup>+</sup> were more readily adsorbed on oxidized molybdenite surfaces, which was in accordance with SEM-EDS results.

In Figure 8d, for pure molybdenite, the peaks at 530.68, 531.85, and 533.20 eV correspond to MoO<sub>2</sub>, MoO<sub>3</sub>, and O<sub>2</sub>/MoS<sub>2</sub> [24]. After oxidation, the three peaks moved to 530.94, 532.06, and 533.55 eV. Meanwhile, the atomic concentration of MoO<sub>3</sub> increased greatly, confirming that the surface oxidation degree increased. After the treatment of DDA, three peaks of unoxidized and oxidized molybdenite also shifted to lower binding energies, which was similar to the S 2p. Since the electronegativity of the O atoms was higher than the S atoms, RNH<sub>2</sub> and RNH<sub>3</sub><sup>+</sup> might adsorb on the O atoms of unoxidized and oxidized molybdenite surface via hydrogen bonding.

### 3.6. Interaction Mechanism

Based on the analysis of Zeta potential, contact angle, SEM-EDS, and XPS, the adsorption mechanism of DDA species on fresh and oxidized faces and edges could be proposed. As illustrated in Figure 9, for fresh faces, RNH<sub>3</sub><sup>+</sup> and RNH<sub>2</sub> interacted with S atoms by hydrogen bonding. For fresh edges, RNH<sub>2</sub> and RNH<sub>3</sub><sup>+</sup> adsorbed on the negatively charged edges via chemical bonding and electrostatic force. On the other hand, for oxidized faces,

$\text{RNH}_2$  and  $\text{RNH}_3^+$  adsorbed on newly exposed S atoms by hydrogen bonding and interacted with oxidized micro-edges through hydrogen bonding and electrostatic forces. For oxidized edges,  $\text{RNH}_2$  and  $\text{RNH}_3^+$  adsorbed on deposited  $\text{MoO}_3$  by hydrogen bonding and electrostatic force.

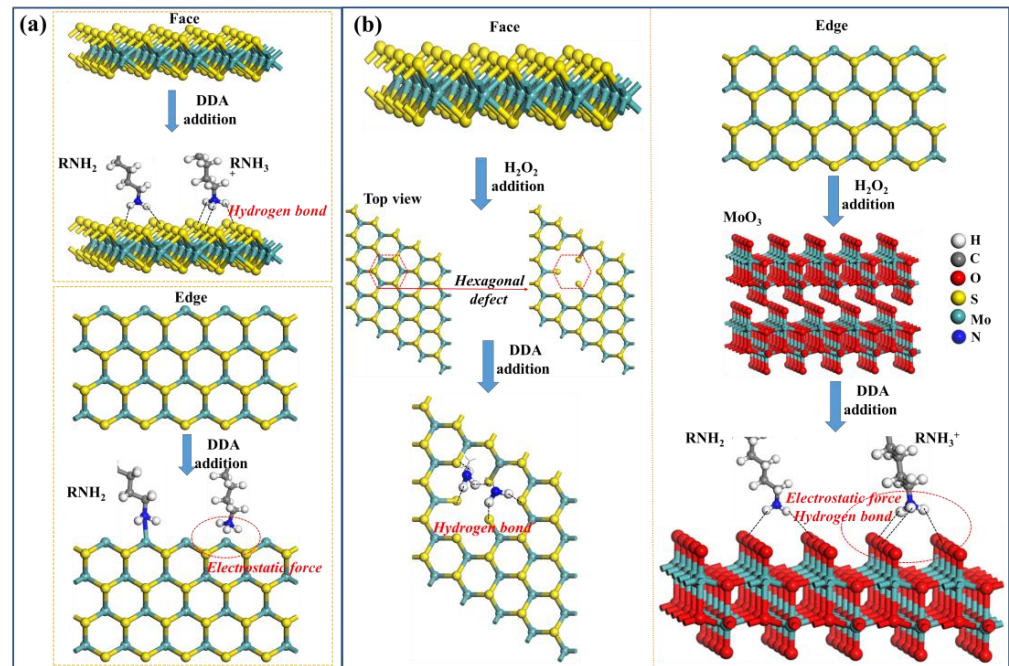


**Figure 9.** The possible interaction mechanism of DDA on molybdenite faces and edges before (a) and after (b) oxidation.

#### 4. Conclusions

- (1) DDA was more efficient than kerosene in the flotation of unoxidized and oxidized molybdenite fines. For unoxidized molybdenite fines, a low dosage of DDA (50 mg/L) achieved a much higher floatability (94.96%) than that (88.56%) obtained at kerosene dosage of 400 mg/L. For oxidized molybdenite fines, the floatability was only 33.62% using 400 mg/L kerosene, while the floatability sharply surged to about 90% at DDA dosage of 100 mg/L. DDA could effectively improve the flotation of unoxidized or oxidized molybdenite fines because of the adsorption of DDA species on both faces and edges.
- (2)  $\text{RNH}_2$  and  $\text{RNH}_3^+$  interacted with S atoms on fresh faces through hydrogen bonding while adsorbed on fresh edges by chemical bonding and electrostatic interaction.
- (3) After oxidation,  $\text{RNH}_2$  and  $\text{RNH}_3^+$  adsorbed on newly exposed S atoms by hydrogen bonding or interacted with  $\text{MoO}_3$  on oxidized micro-edges by hydrogen bonding and electrostatic forces.  $\text{RNH}_2$  and  $\text{RNH}_3^+$  interacted with deposited  $\text{MoO}_3$  on oxidized edges via hydrogen bonding and electrostatic force interaction.

**Author Contributions:** Conceptualization and writing—original draft preparation: B.Y. and J.W.; methodology: H.S. and J.W.; investigation: B.D. and H.S.; visualization and supervision: S.S. and M.Q.; writing-review and editing: B.Y. All authors have read and agreed to the published version of the manuscript.

**Funding:** This research was funded by National Natural Science Foundation of China (grant number: 52074196), Hubei Science Foundation for Distinguished Young Scholars (grant number: 2023AFA047), Technology Innovation Center for Comprehensive Utilization of Strategic Mineral Resources, Ministry of Natural Resources (grant number: CCUM-KY-2309), Consejo Nacional de Humanidades Ciencias y Tecnología (CONAHCYT) of Mexico (grant number: 813204).

**Data Availability Statement:** The raw data supporting the conclusions of this article will be made available by the authors on request.

**Conflicts of Interest:** The authors declare no conflict of interest.

## References

1. Wan, H.; Yi, P.; Song, X.; Luukkanen, S.; Qu, J.; Yang, W.; Li, H.; Bu, X. Role of Improving Molybdenite Flotation by Using Aromatic Hydrocarbon Collector in High-Calcium Water: A Multiscale Investigation. *Miner. Eng.* **2023**, *191*, 107984. [[CrossRef](#)]
2. Li, J.; Deng, W.; Liu, Z.; Pei, B.; Ning, S.; Cai, Z.; Liu, R. Detrimental Effect of Dissolved Natural Organic Matter on Molybdenite Flotation. *Miner. Eng.* **2023**, *193*, 108006. [[CrossRef](#)]
3. Yang, B.; Song, S.; Lopez-Valdivieso, A. Kinetics of Hydrophobic Agglomeration of Molybdenite Fines in Aqueous Suspensions. *Physicochem. Probl. Miner. Process.* **2015**, *51*, 181–189.
4. Wu, J.; Yang, B.; Song, S.; Mildred, Q.; Jia, F.; Tian, X. The Efficient Recovery of Molybdenite Fines Using a Novel Collector: Flotation Performances, Adsorption Mechanism and DFT Calculation. *Miner. Eng.* **2022**, *188*, 107848. [[CrossRef](#)]
5. Wu, J.; Feng, J.; Yang, B.; Martin, R.; Song, S.; Quintana, M.; Jia, F.; Tian, X. The Anisotropic Adsorption of Potassium Cetyl Phosphate on Molybdenite Surface and Its Implication for Improving the Flotation of Molybdenite Fines. *J. Mol. Liq.* **2023**, *378*, 121616. [[CrossRef](#)]
6. Plumlee, G.S.; Ziegler, T.L. *The Medical Geochemistry of Dusts, Soils and Other Earth Materials*, In *Environmental Geochemistry, Treatise on Geochemistry*; Elsevier Ltd.: Oxford, UK, 2005.
7. Fuerstenau, M.C.; Sabacky, B.J. On the Natural Floatability of Molybdenite. *Int. J. Miner. Process.* **1981**, *8*, 79–84. [[CrossRef](#)]
8. Yi, G.; Macha, E.; Van Dyke, J.; Macha, R.E.; McKay, T.; Free, M.L. Recent Progress on Research of Molybdenite Flotation: A Review. *Adv. Colloid Interface Sci.* **2021**, *295*, 102466. [[CrossRef](#)] [[PubMed](#)]
9. Wei, Z.; Li, Y.; Huang, L. New Insight into the Anisotropic Property and Wettability of Molybdenite: A DFT Study. *Miner. Eng.* **2021**, *170*, 107058. [[CrossRef](#)]
10. Lince, J.R.; Frantz, P.P. Anisotropic Oxidation of MoS<sub>2</sub> Crystallites Studied by Angle-Resolved X-Ray Photoelectron Spectroscopy. *Tribol. Lett.* **2001**, *9*, 211–218. [[CrossRef](#)]
11. Song, S.; Zhang, X.; Yang, B.; Lopez-Mendoza, A. Flotation of Molybdenite Fines as Hydrophobic Agglomerates. *Sep. Purif. Technol.* **2012**, *98*, 451–455. [[CrossRef](#)]
12. Wu, J.; Yang, B.; Martin, R.; Song, S.; Quintana, M.; Jia, F.; Luo, H.; Zhou, F.; Tian, X. Anisotropic Adsorption of Xanthate Species on Molybdenite Faces and Edges and Its Implication on the Flotation of Molybdenite Fines. *Miner. Eng.* **2024**, *207*, 108571. [[CrossRef](#)]
13. Gao, Z.; Sun, W.; Hu, Y. New Insights into the Dodecylamine Adsorption on Scheelite and Calcite: An Adsorption Model. *Miner. Eng.* **2015**, *79*, 54–61. [[CrossRef](#)]
14. Jia, F.; Liu, C.; Yang, B.; Song, S. Microscale Control of Edge Defect and Oxidation on Molybdenum Disulfide through Thermal Treatment in Air and Nitrogen Atmospheres. *Appl. Surf. Sci.* **2018**, *462*, 471–479. [[CrossRef](#)]
15. Wang, X.; Zhang, Y.; Si, H.; Zhang, Q.; Wu, J.; Gao, L.; Wei, X.; Sun, Y.; Liao, Q.; Zhang, Z.; et al. Single-Atom Vacancy Defect to Trigger High-Efficiency Hydrogen Evolution of MoS<sub>2</sub>. *J. Am. Chem. Soc.* **2020**, *142*, 4298–4308. [[CrossRef](#)] [[PubMed](#)]
16. Mondal, A.; Paul, A.; Srivastava, D.N.; Panda, A.B. Defect- and Phase-Induced Acceleration of Electrocatalytic Hydrogen Production by Ultrathin and Small MoS<sub>2</sub>-Decorated RGO Sheets. *ACS Appl. NANO Mater.* **2018**, *1*, 4622–4632. [[CrossRef](#)]
17. Fu, Y.; Xiao, Q.; Gao, Y.; Ning, P.; Xu, H.; Zhang, Y. Pressure Aqueous Oxidation of Molybdenite Concentrate with Oxygen. *Hydrometallurgy* **2017**, *174*, 131–139. [[CrossRef](#)]
18. Yang, B.; Yan, H.; Zeng, M.; Zhu, H. Tiopronin as a Novel Copper Depressant for the Selective Flotation Separation of Chalcopyrite and Molybdenite. *Sep. Purif. Technol.* **2021**, *266*, 118576. [[CrossRef](#)]
19. Xu, S.; Kou, J.; Sun, T.; Jong, K. A Study of Adsorption Mechanism of Dodecylamine on Sphalerite. *Colloids Surf. A-Physicochem. Eng. Asp.* **2015**, *486*, 145–152. [[CrossRef](#)]
20. Karas, L.J.; Wu, C.; Das, R.; Wu, J.I. Hydrogen Bond Design Principles. *Wiley Interdiscip. Rev. Comput. Mol. Sci.* **2020**, *10*, e1477. [[CrossRef](#)] [[PubMed](#)]
21. Masatoshi, N.; Jumpei, T.; Shinzo, O. XPS Study of Nitrided Molybdena/Titania Catalyst for the Hydrodesulfurization of Dibenzothiophene. *J. Phys. Chem. B* **1999**, *103*, 10180–10188.
22. Liu, W.; Liu, W.; Dai, S.; Yang, T.; Li, Z.; Fang, P. Enhancing the Purity of Magnesite Ore Powder Using an Ethanolamine-Based Collector: Insights from Experiment and Theory. *J. Mol. Liq.* **2018**, *268*, 215–222. [[CrossRef](#)]
23. Xu, R.; Liu, J.; Sun, W.; Wang, L. Insights into the Synergistic Adsorption Mechanism of Mixed SDS/DDA Collectors on Biotite Using Quartz Crystal Microbalance with Dissipation. *Sep. Purif. Technol.* **2023**, *310*, 123049. [[CrossRef](#)]
24. Suyantara, G.P.W.; Hirajima, T.; Miki, H.; Sasaki, K.; Yamane, M.; Takida, E.; Kuroiwa, S.; Imaizumi, Y. Effect of Fenton-like Oxidation Reagent on Hydrophobicity and Floatability of Chalcopyrite and Molybdenite. *Colloids Surf. A-Physicochem. Eng. Asp.* **2018**, *554*, 34–48. [[CrossRef](#)]

**Disclaimer/Publisher's Note:** The statements, opinions and data contained in all publications are solely those of the individual author(s) and contributor(s) and not of MDPI and/or the editor(s). MDPI and/or the editor(s) disclaim responsibility for any injury to people or property resulting from any ideas, methods, instructions or products referred to in the content.